View metadata, citation and similar papers at core.ac.uk

brought to you by CORE

provided by Open Research Online

Open Research Online

The Open University's repository of research publications and other research outputs

Room temperature thermally evaporated thin Au film on Si suitable for application of thiol self-assembled monolayers in MEMS/NEMS sensors

Journal Item

How to cite:

Mahmoodi, Nasim; Rushdi, Abduljabbar I.; Bowen, James; Sabour, Aydin; Anthony, Carl; Mendes, Paula M. and Preece, Jon A. (2017). Room temperature thermally evaporated thin Au film on Si suitable for application of thiol self-assembled monolayers in MEMS/NEMS sensors. Journal of Vacuum Science and Technology A, 35(4)

For guidance on citations see FAQs.

© 2017 American Vacuum Society

Version: Accepted Manuscript

Link(s) to article on publisher's website:
http://dx.doi.org/doi:10.1116/1.4990026

Copyright and Moral Rights for the articles on this site are retained by the individual authors and/or other copyright owners. For more information on Open Research Online's data policy on reuse of materials please consult the policies page.

oro.open.ac.uk

Room temperature thermally evaporated thin Au film on Si suitable for application of thiol self-assembled monolayers in MEMS/NEMS sensors

Nasim Mahmoodi[a)]
Department of Mechanical Engineering, University of Birmingham, B15 2TT, UK

Abduljabbar Ibrahim Rasheed Rushdi
School of Chemistry, University of Birmingham, B15 2TT, UK

James Bowen
School of Engineering and Innovation, The Open University, MK7 6AA, UK

Aydin Sabouri, Carl J. Anthony
Department of Mechanical Engineering, University of Birmingham, B15 2TT, UK

Paula M. Mendes
School of Chemical Engineering, University of Birmingham, B15 2TT, UK

Jon A. Preece
School of Chemistry, University of Birmingham, B15 2TT, UK

[a)] Electronic mail: n.mahmoodi@bham.ac.uk

Gold is a standard surface for attachment of thiol-based self-assembled monolayers (SAMs). To achieve uniform defect free SAM coatings, which are essential for bio/chemical sensing applications, the gold surface must have low roughness, and be highly orientated. These requirements are normally achieved by either heating during Au deposition or post deposition Au surface annealing. This paper shows that room temperature deposited gold, can afford equivalent gold surfaces, if the gold deposition parameters are carefully controlled. This observation is an important result as heating (or annealing) of the deposited gold can have a detrimental effect on the mechanical properties of the silicon on which the gold is deposited used in microsensors. The paper presents the investigation of the morphology and crystalline structure of Au film prepared by thermal evaporation at room temperature on silicon. The effect of gold deposition rate is studied, and it is shown that by increasing the deposition rate from 0.02 nm s^{-1} to 0.14 nm s^{-1} the gold surface RMS roughness decreases, whereas the grain size of the deposited gold is seen to follow a step function decreasing suddenly between 0.06 and 0.10 nm s^{-1}. The XRD intensity of the preferentially [111] orientated gold crystallites is also seen to increase as the deposition rate increases up to a deposition rate of 0.14 nm s^{-1}. Formation and characterization of 1-dodecanethiol on these Au coated samples is also studied using contact angle. It is shown that by increasing the Au deposition rate the contact angle hysteresis (CAH) decreases until it plateaus, for a deposition rate greater than 0.14 nm s^{-1}, where the CAH is smaller than 9 degrees which is an indication of homogeneous SAM formation, on a smooth surface.

I. INTRODUCTION

Thin gold films are commonly deposited on MEMS/NEMS devices [1-3]. The gold is relatively inert, can be patterned easily and provides a desirable substrate for alkanethiol self-assembled monolayers (SAMs) due to the high affinity between the sulphur of the thiol group and the gold [4, 5]. SAMs are extensively used in a wide range of scientific areas including biosensors and molecular electronics [6-8]. Atomically flat gold substrates are ideal for highly ordered alkanethiol SAMs to minimize the defects in the organic monolayer [5]. Thus, one of the crucial steps in MEMS/NEMS devices utilizing gold/thiol SAMs is to produce a sufficiently flat gold surface.

The properties of the coated gold film have a significant effect on the response of static MEMS/NEMS sensors, such as using cantilever deflection to monitor adsorption of molecules on its surface [9]. Grain boundaries formed as a result of the coalescence of individual gold surface nuclei may cause residual stress [10]. Subsequent molecular adsorption may be affected by this residual stress [9] and the presence of discontinuities in the surface gold structure. The molecular arrangement of a SAM is strongly affected by the morphology of the underlying gold layer [11], therefore, it is crucial to develop a methodology for manufacturing smooth and low stress gold films on silicon substrates for subsequent SAM functionalisation to afford MEMS/NEMS sensors.

One of the common methods to obtain a thin gold film is the thermal evaporation of gold on to a substrate [12-14]. The effect of different parameters such as deposition rate, thickness, pressure, substrate heating and film annealing on the morphology of the deposited gold film on different substrate materials, including silicon, mica and glass, has been investigated previously [12-20]. Studies showed that a deposition rate of less than 1 nm s^{-1} gives a smoother surface [14], the chamber pressure ($<10^{-5}$ Torr) is insignificant compared to other factors [14, 15], the thickness of evaporated gold film has an effect on the size of the island, and [111] plateaus, with lateral dimensions in the range of 200 to 300 nm, occur for film thicknesses greater than 100 nm [17]. Moreover, studies reveal that the substrate temperature during deposition has a great influence on flatness and size of deposited gold grains [12, 14, 15, 18, 19]. By increasing the substrate temperature during deposition, adatoms and surface atoms are in a higher energy state compared to unheated substrate [18]. Therefore, at elevated temperatures sufficient activation energy for adatoms is provided and this enables them to travel longer distances to form a large smooth and continuous plateau, and hence, epitaxy can be enhanced. Reichelt and Lutz showed that for higher deposition rates, higher substrate temperatures are required in order to obtain a well oriented surface and crystal-like film quality [21]. Alternatively, thermal annealing can enhance the flatness of the substrate and can markedly improve the grain size, reduce surface contamination, and afford highly oriented single crystal-like films [16], without the need for heating during deposition. Annealing temperature and time seems not to contribute significantly to surface roughness when compared to other deposition factors [12, 16, 18]. However, annealing or heating of the substrate is not always feasible as it can lead to the generation of undesired stresses in the MEMS/NEMS device. Hence, for MEMS functionalisation high quality gold films deposited at room temperature are highly desirable, therefore, understanding the deposition conditions required to achieve highly crystalline, low roughness gold films is of utmost importance.

In this paper we present the topography (AFM) and structure (XRD) of thermally evaporated gold films deposited at room temperature, as a function of the gold deposition rate. In addition, utilising contact angle hysteresis measurements on SAMS formed from 1-dodecanethiol, we present the study of the effect of gold deposition rate on the quality of the SAM that is subsequently formed on the gold surface. The thin gold film was deposited using deposition rates in the range 0.02-0.18 nm s^{-1}. Si substrates were employed without using any thermal treatment, to avoid unwanted thermally induced stress. Ti was used as an intermediate adhesive

layer between the Au film and Si substrate, as it yields improved crystallinity when compared with chromium [12]. Chromium has also been reported to penetrate though the gold film over time, which leads to concerns over the long-term toxicity of the metal film to biological organisms [5].

II. EXPERIMENTAL

Evaporation was performed using a HHV Auto 306 (HHV Ltd., West Sussex, UK) thermal evaporator. Diced polished 525 μm p-type single crystal Si (100) (IDB Technologies Ltd., Wiltshire, UK) chips (1 cm $\times$ 1 cm) were mounted in the chamber, which was then pumped down to ≈1 μTorr (1.33×10^{-4} Pa). The thickness and deposition rate were monitored using a quartz crystal microbalance (QCM). Ti was used as an adhesive layer between the Au and Si. The deposition materials were placed on the W dimple boat WC1 (HHV Ltd., West Sussex, UK). Following that, the W boat was heated resistively, 5 minutes was allowed for outgassing and after achieving a stable deposition rate the shutter was opened. Ti and Au were sequentially deposited without breaking the vacuum. Ti (99.99%, Kurt J. Lesker) was deposited using a deposition rate of 0.01 ± 0.01 nm s^{-1} to a thickness of 4.0 ± 0.1 nm, following which the Au (99.99%, Kurt J. Lesker) was evaporated using a deposition rate in the range $0.02\text{-}0.18 \pm 0.01$ nm s^{-1} to a thickness of 25.0 ± 0.1 nm.

The morphology of the deposited film surface was studied using a NanoWizard II AFM (JPK Instruments, UK) under ambient conditions. Five different areas were measured on each sample to study the uniformity of the Au coated surface. To investigate the repeatability, three samples with the same deposition rate from different batches were studied. The scan size (500 nm × 500 nm) was kept constant for all the measurements, employing a pixel density of 256×256. Measurements were performed using intermittent mode using a Si cantilever (PPP-NCL, Windsor Scientific, UK) with nominal length, width and thickness 225 ± 10 μm, 38 ± 7.5 μm and 7 ± 1 μm, respectively; tip height and radius were 10-15 μm and <10 nm, respectively.

XRD measurements were conducted using a PANalytical Empyrean Powder X-ray diffractometer, using Cu K_{α} (λ=1.542 Å) X-ray source. Data were collected over the 2-Theta range 30˚ and 100˚ using a 0.02˚ step size.

Exposure of Au coated samples to ambient air results in contamination by volatile organic species in the atmosphere. The procedure to remove this layer from the samples is as follows. Si-chips coated with the adhesion layer of Ti followed by Au were sonicated in HPLC ethanol (Fisher Scientific, UK) for 15 minutes, followed by a 1 h exposure to an oxygen plasma in a UV cleaner (Jelight Company Inc, USA), followed by thorough rinsing with HPLC ethanol. For SAM formation, the Au coated samples were immersed in a 0.1 mM ethanolic solution of dodecanethiol ($HS(CH_2)_{11}CH_3$) (Sigma Aldrich, $\geq$98%, UK) for 24 h. Following that the samples were rinsed with HPLC ethanol to remove unbound thiol, then dried using a stream of nitrogen gas.

The composition of SAM-modified surfaces was investigated using X-ray photoelectron spectroscopy (XPS). Analysis was performed using an Escalab 250 XPS (Thermo Scientific, UK), operating a microfused, monochromated Al Kα X-ray source with a spot diameter of approximately 400 μm. The vacuum pressure in the analysis chamber was < 10^{-7} Pa. Low resolution survey spectra were obtained using a pass energy of 150 eV over a binding energy range of −10 eV to 1200 eV, obtained using 1 eV increments. Recorded low resolution spectra would typically be an average of 5 scans. All high resolution spectra were obtained using a pass energy of 20 eV over a binding energy range of 20–30 eV, centred around a chosen photoelectron binding energy, obtained using 0.1 eV increments. A dwell time of 20 ms was employed when collecting data from each binding energy increment for all measurements. Recorded high resolution spectra would typically be an average of at least 10 scans. CasaXPS software was used for data processing.

The dynamic contact angle measurement was performed using a Theta Lite instrument (KSV Ltd., Helsinki, Finland), equipped with automatic dispensing system. The advancing and receding contact angle of the SAMs were measured using deionized water at 15˚C using the sessile drop technique [22]. The left-hand and right-hand side contact angle was determined using the Young-Laplace equation [23] around the water droplet, and the average value was used for comparison between different samples.

III. RESULTS AND DISCUSSION

The surface topography (AFM) of 25 ± 0.1 nm thickness Au films deposited at different Au deposition rates on Si substrates with an intermediate Ti adhesion layer (4 ± 0.1 nm thickness) are shown in Figure 1. The root-mean-square (RMS) roughness value, R_q, over five different points for each sample were averaged and are reported in Figure 1.

Generally, at all deposition rates the surface consisted of a 'rolling hills' topography which is in-keeping with the studies of Chidsey and Putnam [12, 14]. The Au film is also continuous since the trench depths are small compared to the film thickness, typically no more than 20% of the film thickness.

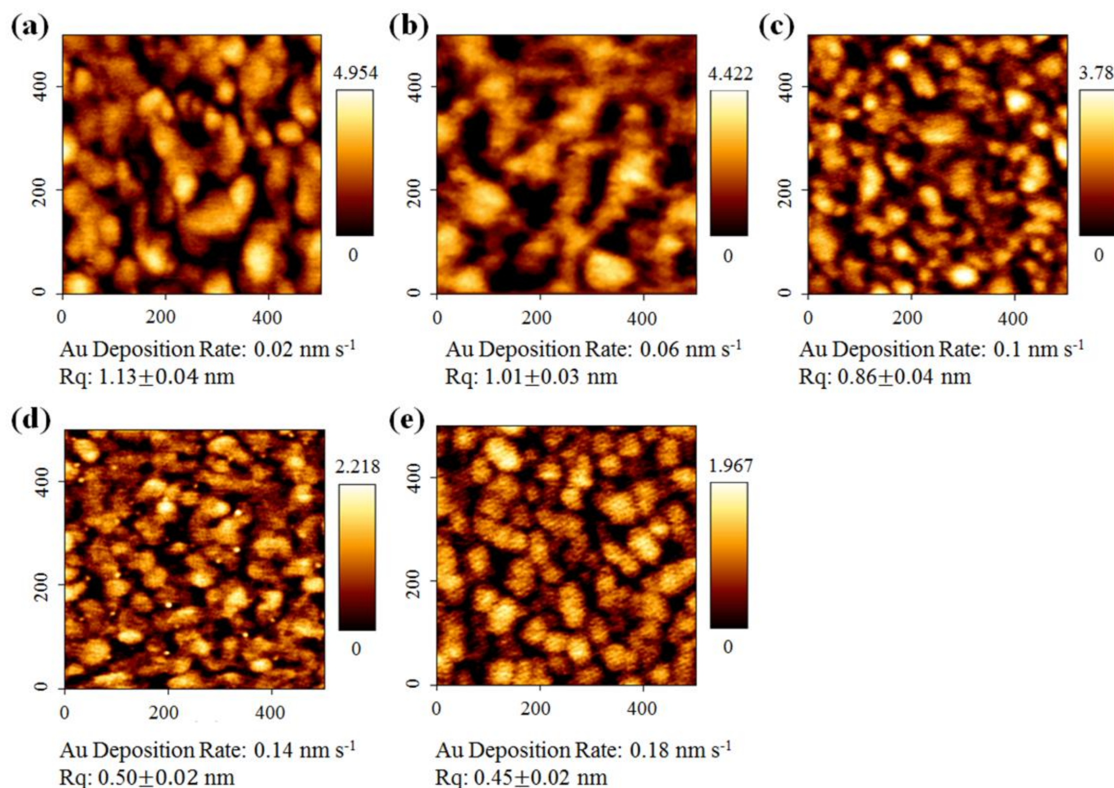

FIG. 1. (Color online) AFM topography images as a function of deposition rate; (a) 0.02 (b) 0.06 (c) 0.10 (d) 0.14 (e) 0.18 nm s-1, and resulting Rq values. Scan size 500 nm × 500 nm and dimension of scale bars are in nm range).

Figure1 (a) shows the topography measurements of the Au film with deposition rate of 0.02 nm s^{-1} and the resulting Rq (1.13nm) is comparable with that reported by Mertens *et al*., whose surfaces exhibited an R_q of 1.60 nm for a deposition rate of 0.02 nm s^{-1} [9]. However, in the Mertens' study a thin Cr film was used as an adhesive layer, relative to this study in which Ti is used. Mertens *et al.* showed that the RMS roughness was dependent on the Au deposition rate decreasing from R_q = 1.60 nm (0.02 nm s^{-1}) to R_q = 1.20 (0.20 nm s^{-1}). Thus, it can be concluded that Ti as an adhesive layer appears to enhance the smoothness of the surface, over Cr. Moreover, other studies have shown that the Cr used as an adhesive layer will diffuse over time into the Au layer, and can change the morphology of the surface [24, 25].

Figure 2 shows that the dimensions of the analysis window chosen for AFM measurements were not found to significantly affect the root-mean-square roughness obtained for the Au film surface topography.

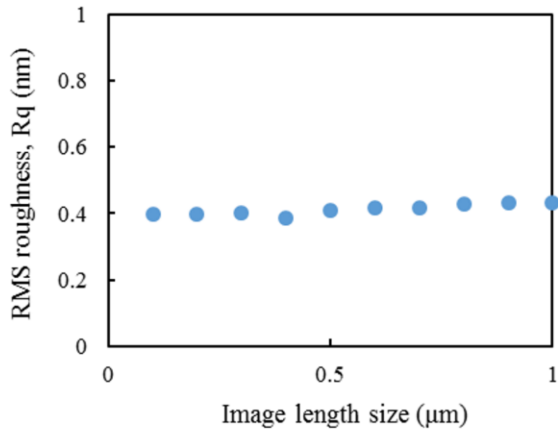

FIG. 2. RMS roughness versus AFM image dimensions.

To check the reproducibility of the deposited Au film, the RMS roughness over three independent preparations using the same deposition conditions were measured. These results are summarized in Figure 3.

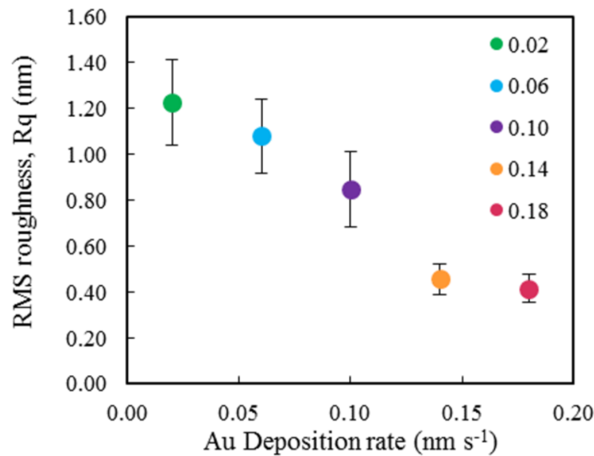

FIG. 3. (Color online) RMS roughness as a function of deposition rate 0.02-0.18 nm/s (each point is a mean value and the error bars represent one standard deviation)

Figure 3 reveals that as deposition rates increase, the RMS roughness Rq value decreases between deposition rates of 0.02-0.14 nm s^{-1}, at which point the decrease has bottomed out.

Figure 1 shows by increasing the deposition rate from 0.02 to 0.06 nm s^{-1}, the grain boundaries become less defined, necking formations occur between adjacent grains and they become more connected (Figure 1(a) and (b)). Upon increasing the deposition rate to 0.10 nm s^{-1} and 0.14 nm s^{-1} (Figure 1(c) and (d)), the lateral dimensions of the grains decrease, as do the peak-to-valley heights. Upon further increasing the deposition rate to 0.18 nm s^{-1} (Figure 1(e)), the grains are more uniformly connected and form isotropic elliptical island. The 3D AFM topographies for deposition rates of 0.02 and 0.18 nm s^{-1} are shown in Figure 4 and the difference between grain size for these deposition rates can be observed; as well as the formation of multigrain islands at the higher 0.18 nm s^{-1} deposition rate.

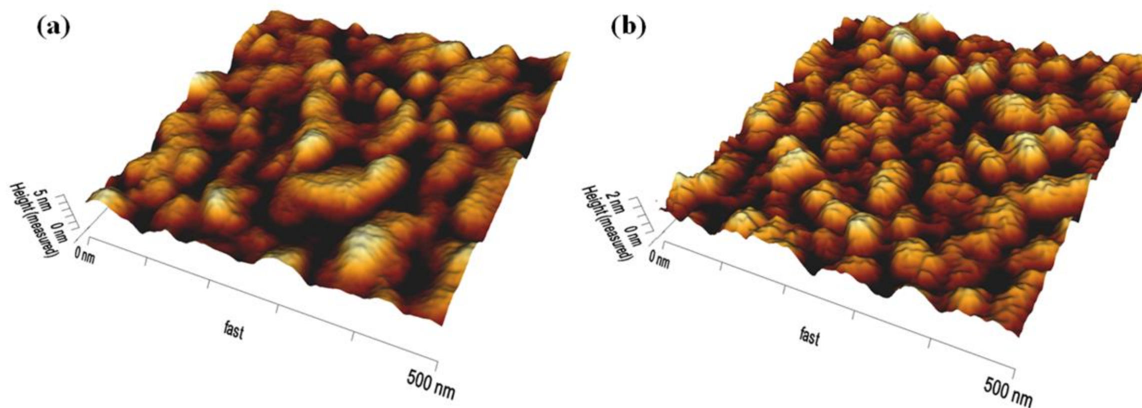

FIG. 4. (Color online) 3D AFM topography for deposition rate (a) 0.02 and (b) 0.18 nm s^{-1}.

Gwyddion open-source software [26] was used for analyzing the grain sizes using AFM images. The Watershed algorithm was implemented to specify the grain boundaries, positions and area. The equivalent average diameters (D_g) based on grain area was calculated for each sample; these results are summarized in Table 1.

TABLE 1. Average lateral grain size (D_g) for different Au deposition rates

Deposition rate (nm s^{-1})	Average grain diameter (D_g, nm)
0.02	85.2±13
0.06	86.7±15.1
0.10	56.2±11.6
0.14	55.4±12.8
0.18	56.1±12.3

The images in Figure 1 and data in Table 1 reveal that a step reduction in the grain size occurs between the deposition rates of 0.06 nm s^{-1} and 0.10 nm s^{-1}. The grain size then remains constant for deposition rates of 0.10-0.18 nm s^{-1}. These results are in agreement with other studies [14, 17, 19]. According to Walton's theory, higher deposition rates lead to an increase in the nucleation rate [27]. Adatoms at lower deposition rates have more time to settle down before other atoms impact on the surface, when compared to a higher deposition rate. At lower deposition rates, the surface diffusion distance also increases and atoms can nucleate and bind to adjacent islands forming larger grains. At higher deposition rates, adatoms agglomerate at binding sites due to arrival of new atoms and so produce smaller grain sizes [28]. These effects are clearly seen in the images of Figure 4, where for the lower deposition rates there are large grains, and for the higher deposition rate, multigrain islands are observed.

XRD was used to study the crystallinity of the Au layer. Figure 5 shows the XRD spectra obtained for Au-coated Si substrates, prepared using Au deposition rates in the range 0.02-0.18 nm s^{-1}; the Au film thickness measured using QCM is 25 ± 0.1 nm for all spectra. For the gold layer the [111] crystal orientation dominated the XRD and the intensity of the diffraction line has a direct relation with the deposition rate. At low deposition rates (0.02 and 0.06 nm s^{-1}) the intensity of the Au[111] diffraction peak is very low, being almost indiscernible for 0.02 nm s^{-1}. It then emerges at deposition rate of 0.10 nm s^{-1}, reaching a maximum at 0.14 nm s^{-1}, and plateauing to 0.18 nm s^{-1}, mirroring the trend in roughness data in Figure 3. Thus, the film

crystallinity increases with higher deposition rates. It is worth noting that the X-ray diffraction was collected using a Cu Kα source with two wavelengths; $CuK_{\alpha1}$ and $CuK_{\alpha2}$ with almost identical wavelength of 1.5406 and 1.5444 Å, respectively. Based on Bragg's law, d=nλ/(2sin(θ)), two peaks can be generated within the same reflection at these wavelengths. This effect is enhanced at higher reflection angles and explains the two peaks for Si (100) [27]. The XRD measurements were also performed on uncoated Si samples and it was confirmed that the peaks at ~38º and 82º were only due to the substrate's coatings and so could be attributed to the Au [111] and [222] orientations.

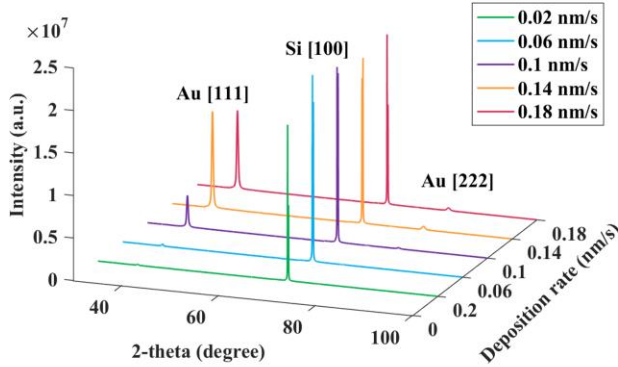

FIG. 5. (Color online) X-ray diffraction of Au coated samples produced using deposition rates in the range 0.02-0.18 nm/s.

The mean crystal size, D_P, was determined from XRD data using the Scherrer formula [29]:

$$D_P = \frac{0.9\lambda}{\beta_P \cos\theta} \qquad (1)$$

Where β_p is the full width at half maximum (FWHM) due to particle size, θ is the diffraction angle, and λ is the X-ray wavelength.

Figure 6 presents the mean grain size (D_g) from AFM data and crystal size normal to [111] plane from XRD data using Scherrer formula.

By increasing the deposition rate the diffraction peak intensity enhanced, while βp and hence D_p remain almost identical, which is an indication of improving film crystallinity. It can be concluded that higher deposition rates lead to a larger proportion of the film with a preferred [111] orientation. The D_g and D_p from AFM and XRD, respectively, confirm that the lateral grain size and crystal size normal to [111] plane remain almost constant for deposition rates 0.1-0.18 nm s^{-1}. The number of grains is almost constant for these deposition rates and higher XRD intensity means the film crystallinity has been promoted and more grains become [111] crystalline.

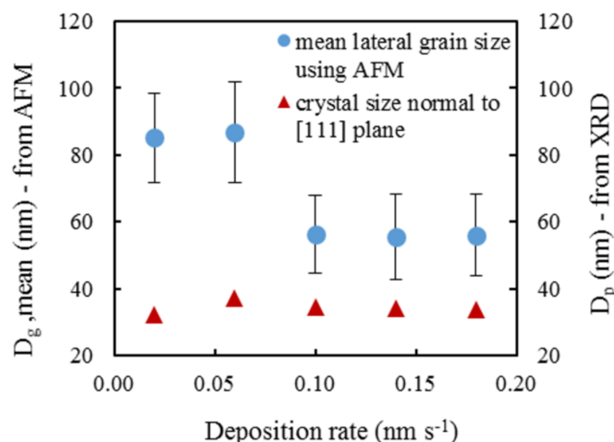

FIG. 6. (Color online) (a) Dp and Dg versus deposition rate.

Figure 7 shows the S 2p photoelectron spectrum obtained from XPS measurements, indicating that the SAM has chemisorbed successfully on the Au surface.[30]

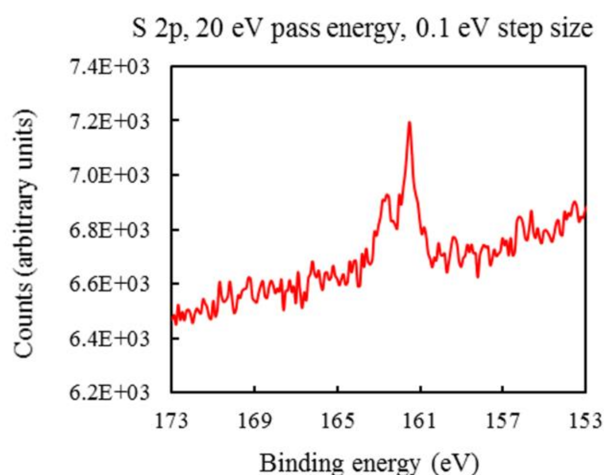

FIG. 7. XPS spectra of the S 2p photoelectrons from 1-dodecanethiol monolayer on gold.

Contact angle measurements were used to assess the homogeneity and organization of the SAMs. The advancing and receding contact angle, Φa and Φr, respectively, of a SAM formed from 1-dodecanethiol on Au coated samples with different Au deposition rates in the range 0.02-0.18 nm s^{-1} were measured on three different places of each sample.

The contact angle hysteresis (CAH), which is a difference between the advancing and receding contact angles, is an indication of homogeneity of SAM. It is useful to have an accurate measure of the actual influence of surface roughness on the CAH for a given SAM system (Figure 8). For the samples investigated here the CAH is larger for Au films produced at lower deposition rates (0.02, 0.06 and 0.10 nm s^{-1}, whilst the two faster deposition rates have a lower CAH, which is in-keeping with the accepted convention that CAH increases with surface roughness. For deposition rates greater than 0.14 nm s^{-1} the CAH is smaller than 9 degrees which is an indication of homogenous SAM formation. The measured Φa and Φr values were also consistent with the results of Evans *et al.* (Φa =110˚) and Laibinis *et al.* (Φa =116˚ and Φr =102˚) [31, 32].

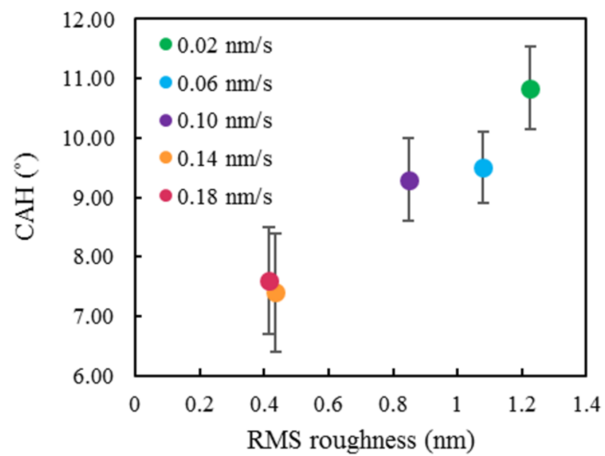

FIG. 8. (Color online) CAH versus RMS roughness.

IV. SUMMARY AND CONCLUSIONS

This paper presents a study of the quality of Au films manufactured using thermal evaporation onto Si substrates at room temperature. The Au films were then assessed for their suitability as substrates for the deposition of self-assembled monolayers. Firstly, the morphology of the deposited Au film on a Si substrate with Ti as an adhesive layer as a function of deposition rate was studied using AFM, which yielded lower roughness at higher deposition rates. The average grain size remains constant for deposition rates 0.02-0.06 nm s^{-1}, a step in grain size occurs at 0.06 nm s^{-1} and remains almost identical for deposition rate 0.1-0.18 nm s^{-1}. The effect of deposition rate on Au film crystallinity was then studied using XRD, the data revealing a Au film with the preferential [111] orientation with respect to the substrate surface. The highest crystallinity was observed for films manufactured using a deposition rate of 0.14 nm/s.

The effect of Au deposition rate, i.e. surface morphology, on the properties of 1-dodecanethiol SAMs was investigated. It was observed that by increasing the deposition rate, SAMs become more homogenous and well-ordered, and the hysteresis between advancing and receding contact angle decreases.

In general, at higher deposition rates, the RMS roughness decreases, [111] crystal quality is enhanced, and alkanethiol SAMs become more well-ordered. The applications of thin Au films on Si substrates for various types of MEMS/NEMS structures, biosensors, electronics - to name but a few - attracts significant interest, and it is clear that suitable Au films deposited on unheated substrates can be obtained for these applications by varying the deposition conditions.

ACKNOWLEDGMENTS

The JPK Instruments NanoWizard II AFM and PANalytical Empyrean Powder X-ray diffractometer used in this research were obtained through Birmingham Science City: Innovative Uses for Advanced Materials in the Modern World (West Midlands Centre for Advanced Materials Project 2) and Creating and Characterising Next Generation Advanced Materials (West Midlands Centre for Advanced Materials Project 1), respectively, with support from Advantage West Midlands (AWM) and part funded by the European Regional Development Fund (ERDF). Mendes acknowledges the support of EPSRC (EP/K027263/1) and ERC (Consolidator Grant 614787).

REFERENCES

[1]A. Boisen, S. Dohn, S. S. Keller, S. Schmid and M. Tenje, Rep. Prog. Phys. **74** (3), 036101 (2011).
[2]F. Bosco, M. Bache, J. Yang, C. Chen, E.-T. Hwu, Q. Lin and A. Boisen, Sensor. Actuat. A-Phys. **195**, 154-159 (2013).
[3]S. Sang, Y. Zhao, W. Zhang, P. Li, J. Hu and G. Li, Biosens. Bioelectron. **51**, 124-135 (2014).
[4]Y.-K. Hong, H. Yu, T. G. Lee, N. Lee, J. H. Bahng, N. W. Song, W. Chegal, H. K. Shon and J.-Y. Koo, Chem. Phys. **428**, 105-110 (2014).
[5]J. C. Love, L. A. Estroff, J. K. Kriebel, R. G. Nuzzo and G. M. Whitesides, Chem. Rev. **105** (4), 1103-1170 (2005).
[6]D. Aswal, S. Lenfant, D. Guerin, J. Yakhmi and D. Vuillaume, Anal. Chim. Acta **568** (1), 84-108 (2006).
[7]I.-Y. Huang and M.-C. Lee, Sensor Actuat. B-Chem. **132** (1), 340-348 (2008).
[8]M. Alvarez and L. M. Lechuga, Analyst **135** (5), 827-836 (2010).
[9]J. Mertens, M. Calleja, D. Ramos, A. Tarýn and J. Tamayo, J. Appl. Phys. **101** (3), 034904 (2007).
[10]S. Arcidiacono, N. Bieri, D. Poulikakos and C. Grigoropoulos, Int. J. Multiphas. Flow **30** (7), 979-994 (2004).
[11]M. Godin, P. Williams, V. Tabard-Cossa, O. Laroche, L. Beaulieu, R. Lennox and P. Grütter, Langmuir **20** (17), 7090-7096 (2004).
[12]C. E. Chidsey, D. N. Loiacono, T. Sleator and S. Nakahara, Surf. Sci. **200** (1), 45-66 (1988).
[13]C. Nogues and M. Wanunu, Surf. Sci. **573** (3), L383-L389 (2004).
[14]A. Putnam, B. Blackford, M. Jericho and M. Watanabe, Surf. Sci. **217** (1-2), 276-288 (1989).
[15]J. DeRose, T. Thundat, L. Nagahara and S. Lindsay, Surf. Sci. **256** (1), 102-108 (1991).
[16]M. H. Dishner, M. M. Ivey, S. Gorer, J. C. Hemminger and F. J. Feher, J. Vac. Sci. Technol. A **16** (6), 3295-3300 (1998).
[17]M. Levlin, A. Laakso, H.-M. Niemi and P. Hautojärvi, Appl. Surf. Sci **115** (1), 31-38 (1997).
[18]Z. H. Liu, N. M. Brown and A. McKinley, J. Phys-Condens. Mat. **9** (1), 59 (1997).
[19]N. Semaltianos and E. Wilson, Thin Solid Films **366** (1), 111-116 (2000).
[20]V. Švorčík, O. Kvitek, J. Říha, Z. Kolska and J. Siegel, Vacuum **86** (6), 729-732 (2012).
[21]K. Reichelt and H. Lutz, J. Cryst. Growth **10** (1), 103-107 (1971).
[22]S. Srinivasan, G. H. McKinley and R. E. Cohen, Langmuir **27** (22), 13582-13589 (2011).
[23]Y. Yuan and T. R. Lee, in *Surface science techniques* (Springer, 2013), pp. 3-34.
[24]M. George, W. Glaunsinger, T. Thundat and S. Lindsay, Thin solid films **189** (1), 59-72 (1990).
[25]N. Moody, D. Adams, D. Medlin, T. Headley, N. Yang and A. Volinsky, Int. J. Fracture **120** (1-2), 407-419 (2003).
[26]M. Fan, C. Huang, A. E. Bland, Z. Wang, R. Slimane and I. G. Wright, *Environanotechnology*. (Elsevier, 2010).
[27]J. D. Rachwal, X-ray diffraction applications in thin films and (100) silicon substrate stress analysis (2010).
[28]Y. Golan, L. Margulis, S. Matlis and I. Rubinstein, J. Electrochem. Soc. **142** (5), 1629-1633 (1995).
[29]U. Holzwarth and N. Gibson, Nat. Nanotechnol. **6** (9), 534-534 (2011).
[30]C. D. Bain, H. A. Biebuyck, G. M. Whitesides, Langmuir 5 (3), 723-727 (1989).
[31]S. D. Evans, R. Sharma and A. Ulman, Langmuir **7** (1), 156-161 (1991).
[32]P. E. Laibinis, G. M. Whitesides, D. L. Allara, Y. T. Tao, A. N. Parikh and R. G. Nuzzo, J. Am. Chem. Soc. **113** (19), 7152-7167 (1991).